A ∼6 Mpc overdensity at z ∼2.7 detected along a pair of quasar sight lines: filament or protocluster?

Hayley Finley, Patrick Petitjean, Pasquier Noterdaeme, Isabelle Pâris

**Astronomy
&
Astrophysics**

A ∼6 Mpc overdensity at $z \simeq 2.7$ detected along a pair of quasar sight lines: filament or protocluster?[⋆]

Hayley Finley[1], Patrick Petitjean[1], Pasquier Noterdaeme[1], and Isabelle Pâris[2]

[1] Institut d'Astrophysique de Paris, CNRS-UPMC, UMR7095, 98bis bd Arago, 75014 Paris, France
    e-mail: finley@iap.fr
[2] INAF – Osservatorio Astronomico di Trieste, via G. B. Tiepolo 11, 34131 Trieste, Italy

ABSTRACT

Simulations predict that gas in the intergalactic medium (IGM) is distributed in filamentary structures that connect dense galaxy clusters and form the cosmic web. These structures of predominantly ionized hydrogen are difficult to observe directly due to their lack of emitting regions. We serendipitously detected an overdensity of log N(H I) > 18.0 absorbers at $z \simeq 2.69$ along the lines of sight toward a pair of background quasars. Three main absorption regions spanning ∼2000 km s^{-1} (corresponding to 6.4 h_{70}^{-1} Mpc proper) are coincident in the two lines of sight, which are separated by ∼90 h_{70}^{-1} kpc transverse proper distance. Two regions have [Fe/H] < −1.9 and correspond to mild overdensities in the IGM gas. The third region is a sub-DLA with [Fe/H] = −1.1 that is probably associated with a galaxy. We discuss the possibility that the lines of sight probe along the length of a filament or intercept a galaxy protocluster.

Key words. quasars: absorption lines – intergalactic medium – large-scale structure of Universe

1. Introduction

Filamentary structures that emerge both from the large-scale distribution of galaxies and in cosmological simulations are iconic for the cosmic web (Bond et al. 1996). Filaments and sheets outline vast, extremely underdense regions known as voids, before meeting at nodes that coincide with matter-rich galaxy clusters. Various techniques are used to identify structures in cosmological simulations and trace filaments (e.g., Bond et al. 2010; Murphy et al. 2011; Sousbie et al. 2011; Smith et al. 2012; Cautun et al. 2014), the longest of which span more than 100 h^{-1} Mpc. Segments connecting two clusters are relatively straight with typical lengths of 5−20 h^{-1} Mpc and radial profiles that fall off beyond 2 h^{-1} Mpc (Colberg et al. 2005; González & Padilla 2010; Aragón-Calvo et al. 2010).

At low redshift, filament finding techniques applied to the Sloan Digital Sky Survey (SDSS; York et al. 2000) galaxy distribution measure maximum lengths comparable to simulations: 60−110 h^{-1} Mpc (Pandey et al. 2011; Tempel et al. 2014). The majority of galaxies lie within 0.5 h^{-1} Mpc of the filament axis (Tempel et al. 2014). Another strategy is to look for evidence of filamentary structures that connect a particular galaxy cluster to the cosmic web. Observations of clusters at $z \sim 0.5$ reveal that they are embedded in filaments extending more than 14 h^{-1} Mpc (Tanaka et al. 2007; Verdugo et al. 2012). Complimentary to using galaxies as tracers, filaments can also be directly detected from weak gravitational lensing signals (Mead et al. 2010). Jauzac et al. (2012) unambiguously identify a filament with projected length ∼3.3 h^{-1} Mpc (3D length 13.3 h^{-1} Mpc) feeding into a massive galaxy cluster at $z = 0.55$.

At high redshift, diffuse H I in the intergalactic medium (IGM) imprints absorptions in the spectra of background quasars and creates the Lyman-alpha (Lyα) forest. Correlations on scales <5 h^{-1} Mpc comoving in the Lyα forests of quasar lines of sight (LOSs) with small angular separations (e.g., D'Odorico et al. 1998; Rollinde et al. 2003; Coppolani et al. 2006; D'Odorico et al. 2006; Saitta et al. 2008; Cappetta et al. 2010) likely arise from filaments. Reconstruction methods applied to simulated and observed IGM absorptions recover the topology of this low-density gas at $z \sim 2$ (Caucci et al. 2008; Cisewski et al. 2014). However, little is known observationally about the topology of the IGM, and the actual H I gas distribution may be less filamentary than simulated structures (Rudie et al. 2012). Currently, the source density limits our ability to resolve cosmic web filaments. Lee et al. (2014) suggest that observing programs with existing 8−10 m telescopes could achieve the source density necessary to obtain a resolution of ∼3−4 h^{-1} Mpc over cosmologically interesting volumes. However, the next generation of 30 m-class telescopes will best address the challenge of resolving filaments (Steidel et al. 2009; Maiolino et al. 2013; Evans et al. 2014).

It is clear from these studies that quasar LOSs intersect structures in the cosmic web. While they most often pass through the filament width, certain LOSs foreseeably probe along the length. Here we present H I absorptions indicative of the gaseous environment within a filament. We detect multiple, consecutive absorptions at $z \simeq 2.69$ with log N(H I) (cm^{-2}) > 18.0 that span nearly 2000 km s^{-1} and are coincident in *both* LOSs toward a pair of quasars separated by about 11″.

We describe the quasar spectra in Sect. 2, including how the close LOS pair was identified, and analyze the absorptions in each LOS in Sect. 3. In Sect. 4, we discuss evidence for whether the LOSs intercept a galaxy protocluster or probe along

---

[⋆] Based on observations with X-shooter on the Very Large Telescope at the European Southern Observatory under program 089.A-0855.

Table 1. Column densities [$\log(N/\mathrm{cm}^{-2})$] for components of the $\log N(\mathrm{H\,I}) = 20.2$ cm^{-2} sub-DLA detected in the BG quasar LOS.

z	v	O I	$\sigma_{\mathrm{O\,I}}$	Si II	$\sigma_{\mathrm{Si\,II}}$	C II	$\sigma_{\mathrm{C\,II}}$	Al II	$\sigma_{\mathrm{Al\,II}}$	Al III	$\sigma_{\mathrm{Al\,III}}$	Fe II	$\sigma_{\mathrm{Fe\,II}}$
2.687165	−180	14.52:	0.04	13.31	0.08	14.75:	0.11	12.22	0.06	11.69	0.35	12.95	0.05
2.688148	−100	15.09:	0.02	14.17	0.02	14.92:	0.03	12.90	0.03	11.93	0.29	13.73	0.01
2.688912	−38	16.23:	0.33	14.11	0.04	15.10:	0.44	13.35	0.10	12.21	0.13	14.16	0.03
2.689329	−4	17.59:	0.44	14.72	0.07	14.61:	0.66	12.95	0.06	12.09	0.17	13.74	0.03
2.689953	47	14.89:	0.03	14.04	0.02	15.07:	0.03	12.76	0.03	11.57	0.90	13.58	0.02
2.692830	280	14.16	0.03	13.44	0.06	14.19	0.02	12.23	0.05	–	–	13.06	0.04

Notes. Velocities (km s^{-1}) are relative to the BG-C system redshift, $z = 2.6894$. The main components of both O I and C II are saturated.

the length of a filament. We use a ΛCDM cosmology with $\Omega_\Lambda = 0.73$, $\Omega_{\mathrm{m}} = 0.27$, and $H_0 = 70$ km s^{-1} Mpc^{-1} (Komatsu et al. 2011).

2. Data

The targeted quasars relevant to this work are SDSS J091338.30-010708.7 at $z \sim 2.75$ ($r = 20.49$) and J091338.96-010704.6 at $z \sim 2.92$ ($r = 20.38$). We refer to them as the foreground (FG) and background (BG) quasar accordingly. Their angular separation is 10.74″, which corresponds to 87.8 h_{70}^{-1} kpc proper distance (0.32 h_{70}^{-1} Mpc comoving) at $z = 2.69$. These quasars were identified in the publicly available data release 9 quasar catalog (DR9Q; Pâris et al. 2012) from the SDSS-III (Eisenstein et al. 2011) Baryon Oscillation Spectroscopic Survey (BOSS; Dawson et al. 2013).

Initial interest in the pair was due to a damped Lyα absorption (DLA) in the BG LOS at the redshift of FG quasar, which offers an opportunity to study the host galaxy environment in absorption (Finley et al. 2013, and in prep.). In the low-resolution BOSS spectrum, an additional DLA with $\log N(\mathrm{H\,I}) = 21.05$ at $z_{\mathrm{abs}} = 2.680$ is flagged in the BG LOS (Noterdaeme et al. 2012b). A corresponding system appears in the FG BOSS LOS, but the low column density excludes it from the catalog of $\log N(\mathrm{H\,I}) \geq 20$ absorbers. Motivated by the absorption systems, we pursued a higher resolution analysis of these LOSs.

The quasars were observed in service mode in spring 2013 with X-shooter on the 8.2 m Kueyen (UT2) telescope at the European Southern Observatory as part of a program (ESO 089.A-0855, P.I. Finley) targeting non-binary quasar pairs with small angular separations. The X-shooter spectrograph has UVB, VIS, and NIR arms that allow simultaneous observations across the full wavelength range from 300 nm to 2.5 μm. The total exposure times were 2×3000 s (1.67 h) for the FG quasar and 5×3720 s (5.17 h) for the BG quasar.

The data were reduced with version 2.2.0 of the ESO X-shooter pipeline (Modigliani et al. 2010). The bias level for the raw UVB and VIS frames was corrected by calculating the bias from the overscan region. Cosmic rays in the science exposures were flagged with the van Dokkum (2001) Laplacian edge detection method. After background subtraction, the science exposures were divided by the master flat for the appropriate arm, created from flat frames taken during the same day of observations. Sky emission lines were then subtracted using the technique from Kelson (2003). Each spectral order was rectified from image space to wavelength space, using the 2D wavelength solution obtained from calibration frames. The individual 2D orders were extracted and merged, with pixel values weighted by the inverse variance of the corresponding errors in the overlapping regions. 1D spectra were obtained via standard extraction in the pipeline.

The extracted 1D spectra from different exposures were shifted to the vacuum-heliocentric reference frame and combined with an inverse variance weighted average. As in Noterdaeme et al. (2012a), we correct a 0.2 Å shift between the UVB and VIS spectra. The signal-to-noise ratio is 47 (21) at 5350 Å and 38 (15) at 8100 Å in the BG (FG) spectrum. We find that the resolution in the VIS spectra ($R \approx 11\,000$), measured from the width of telluric absorption lines, is higher than the nominal resolution ($R = 8800$), since the seeing was smaller than the 0.9″ slit width. The resolution in the UVB (1.0″ slit width) is likewise approximately $R \approx 6400$.

3. Absorption systems

We identify consecutive intervening H I absorptions spanning $\Delta v \simeq 2000$ km s^{-1} at $z \simeq 2.69$ that are coincident in both LOSs toward the J0913-0107 non-binary quasar pair. A proper distance of ~ 90 h_{70}^{-1} kpc at this redshift separates the FG and BG quasar LOSs. Three main absorption regions are denoted A, B, and C in the two spectra (Fig. 1). We fit the entire absorption structure with the VPFIT package[1] to obtain system redshifts and column densities for the components (Fig. 2). Seven absorptions have $\log N(\mathrm{H\,I})$ (cm^{-2}) > 18.0, and we refer to them by the LOS, absorption region, and component number: BG-A1, BG-A2, BG-B, BG-C, FG-A1, FG-A2, and FG-B. We discuss the absorption systems in each LOS.

3.1. Background quasar line of sight

3.1.1. H I absorption systems

The H I absorption profiles for the components in regions A, B, and C are constrained from fitting Lyα–Lyδ in the UVB spectrum (Fig. 2, left). The redshifts for components BG-A1 ($z = 2.6688$), BG-A2 ($z = 2.6718$), and BG-C ($z = 2.6894$) are fixed based on the fits to their associated low-ionization metal transitions (Fig. 4). The absorption in region C is a $\log N(\mathrm{H\,I}) = 20.2 \pm 0.1$ sub-DLA, and the associated metals are fitted with six components. The main absorption, with five components, spans ~ 225 km s^{-1}, and the sixth component at 280 km s^{-1} is redshifted relative to the $z = 2.6894$ system redshift. The BG-C redshift is the average of the six components weighted by their Fe II column densities, which are given in Table 1.

The flux in the vicinity of Lyα is almost completely absorbed, except for a small peak separating region A from regions B and C at −950 km s^{-1}. Components BG-A1 and BG-A2 are both sub-DLAs, with $\log N(\mathrm{H\,I}) = 19.9 \pm 0.1$ and 19.7 ± 0.3 respectively. Strong Si II $\lambda\lambda1190$, 1193 absorptions from a $z \simeq 2.75$ DLA blend with the H I absorptions and contribute to the
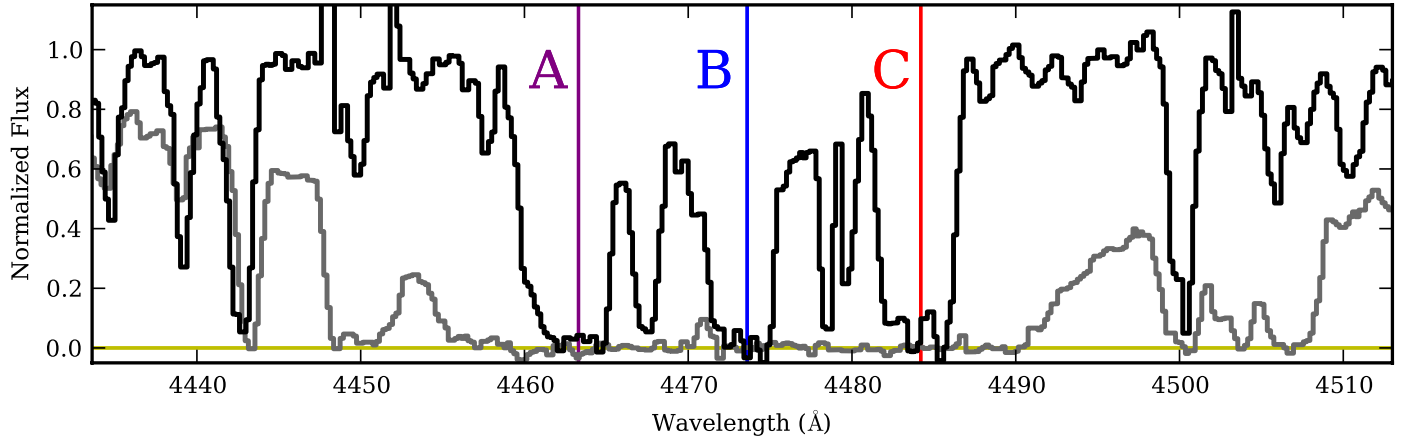
---

[1] http://www.ast.cam.ac.uk/~rfc/vpfit.html

Fig. 1. Portion of the Lyα forest with significant, coincident H I absorptions along both LOSs. The FG spectrum (black) is overplotted on the BG spectrum (gray). The main absorption regions are labelled A (purple), B (blue), and C (red).
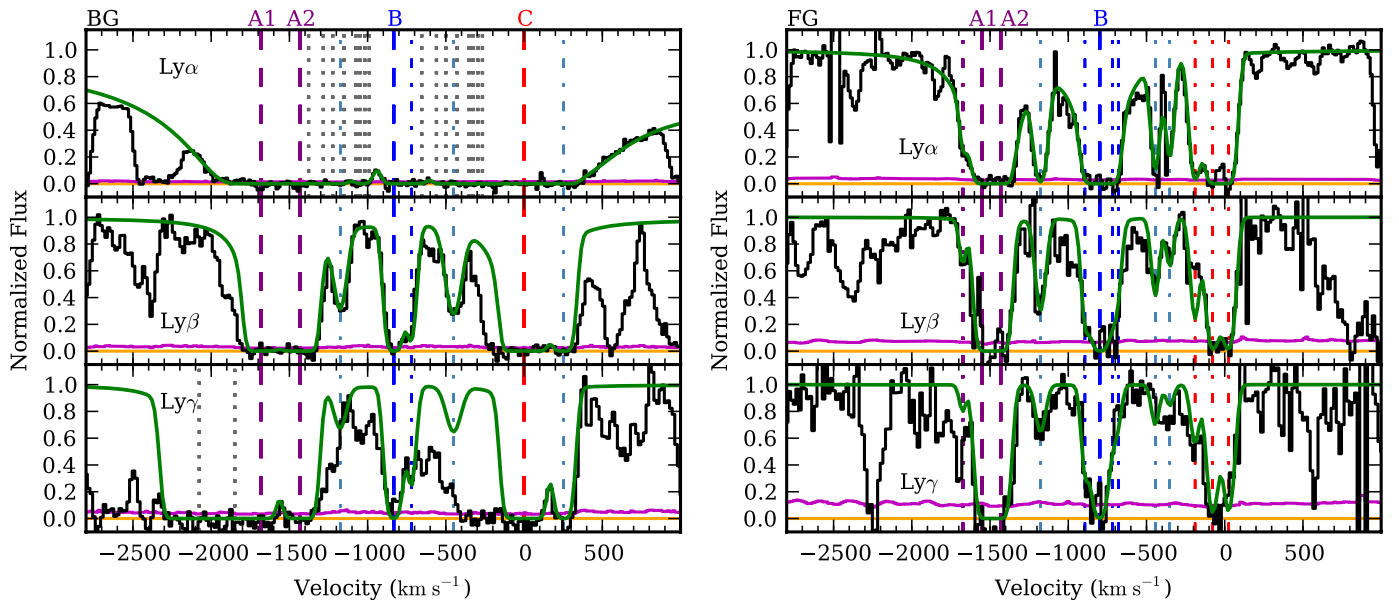

Fig. 2. Fits to Lyα (*top*), Lyβ (*middle*), and Lyγ (*bottom*) H I absorptions in the BG (*left*) and FG (*right*) spectra. Dashed purple, blue, and red lines mark the log N(H I) > 18.0 components in regions A, B, and C, while dash-dotted purple, blue, and red lines indicate the weaker components within the respective regions. Dash-dotted blue-gray lines signal low column density components between the three main regions that are also part of the absorption structure. Dotted gray lines in the BG-Lyα panel indicate blended components from Si II $\lambda\lambda$1190, 1193 absorptions associated with a $z \simeq 2.75$ DLA. Zero velocity is relative to the BG-C system redshift, $z = 2.6894$, and the 1-σ error on the flux is shown in magenta.

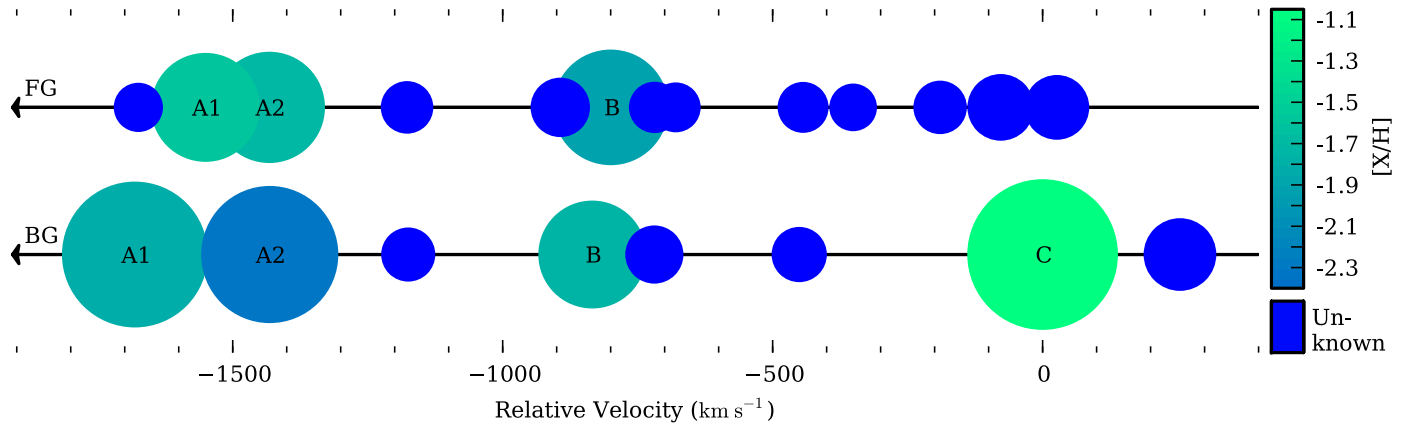**Fig. 3.** Diagram of H I clouds distributed along the FG and BG quasar LOSs. Circle sizes scale with the H I column density such that twice the area represents eight times as much N(H I) (Area = N(H I)$^{1/3}$). Low column density clouds, for which no metallicity is measured, are dark blue, while brighter, greener colors indicate clouds with higher metallicities. Zero velocity is at $z = 2.6894$.

Table 2. H I column densities [log (N/cm^{-2})] for components along the BG and FG quasar LOSs.

Comp. Name	v (km s^{-1})	BG log N(H I)	FG log N(H I)
BG-A1	−1681	19.90	–
	−1675	–	14.32
FG-A1	−1550	–	18.46
BG-A2, FG-A2	−1432	19.67	18.57
	−1176	14.82	14.66
	−893	–	15.30
BG-B	−834	18.41	–
FG-B	−800	–	18.77
	−719	15.20	14.54
	−680	–	14.39
	−451	14.92	–
	−444	–	14.50
	−351	–	14.15
	−190	–	14.75
	−78	–	15.90
BG-C	0	20.15	–
	26	–	15.75
	294	16.22	–

Notes. Velocities (km s^{-1}) are relative to the BG-C system redshift, $z = 2.6894$.

extended zero-level flux. The components in region B are more apparent in the Lyβ profile, and when they are included the fit to Lyα recovers the small peak near −950 km s^{-1}. The strong component labelled BG-B (Fig. 2, left) is a log N(H I) = 18.4 ± 0.2 Lyman limit system (LLS). All eight H I absorptions fitted in the BG spectrum are listed with their velocity offsets relative to the BG-C component in Table 2.

3.1.2. Abundances

Table 3 gives abundances for the LLS and sub-DLA systems in the three regions. The abundances are calculated with respect to solar values (Lodders 2003) following the convention [X/H] ≡ log (X/H) − log (X/H)$_\odot$.

The BG-A1 and BG-A2 metal absorptions are single-component, and we detect O I, which is a good indicator of the metallicity. Charge transfer processes imply that O I and H I are tightly related (Field & Steigman 1971). Since both the O I λ1302 and O I λ1039 transitions are detected for the BG-A1 component, the absorption line fit is well-constrained. The oxygen abundance is [O/H] = −1.19 ± 0.34. The Si, Al, and Fe abundances are slightly lower with [X/H] = −1.7, −2.1, and −1.9 respectively. The BG-A1 C II λ1334 absorption is blended with Si II λ1304 from the $z = 2.75$ DLA. We estimate the de-blended C abundance, [C/H] = −1.83 ± 0.59, by fixing the DLA N(Si II) from other transitions and imposing the same FWHM as for the other BG-A1 absorptions.

The O I λ1039 transition is blended for the BG-A2 component, but the absorptions are non-saturated. The oxygen abundance, [O/H] = −1.56 ± 0.43, is again slightly higher than the Si, C, Al, and Fe abundances [X/H] ≲ −2.1. The BG-A2 C II λ1334 absorption is redder than the DLA Si II λ1304 absorption and unaffected by blending.

The [C/O] values, −0.64 ± 0.68 for BG-A1 and −0.54 ± 0.55 for BG-A2, follow the trend where, in low-metallicity systems, [C/O] increases as [O/H] decreases (Cooke et al. 2011; Dutta et al. 2014).

No metal transitions corresponding to the H I absorptions in region B are detected (Fig. 4) to a limit of log N(O I) ≤ 13.0 ± 0.1. To obtain this estimate, we use the average FWHM from the detected BG-A1 and BG-A2 O I components and limit the absorption strength according to the noise in the flux. The upper limit on the [O/H] abundance is −1.80 ± 0.25.

The abundances for the region C sub-DLA, [Si/H] = −0.71 ± 0.11, [Al/H] = −0.89 ± 0.08, and [Fe/H] = −1.13 ± 0.18, are somewhat higher than the average value for intervening DLAs at $z \simeq 2.69$, ⟨Z⟩ = −1.24 ± 0.12 (Rafelski et al. 2012). The enhanced [Si/Fe] value, = 0.41 ± 0.21, is typical of intervening DLAs at this redshift and is likely due to dust depletion (Prochaska & Wolfe 2002; Vladilo 2002). Absorptions BG-A1, BG-A2, and BG-B all have abundances approximately an order of magnitude lower than that of BG-C.

3.2. Foreground quasar line of sight

3.2.1. H I absorption systems

H I absorptions in the FG quasar Lyα forest have a structure similar to the systems in the same redshift range in the BG quasar spectrum (Fig. 1). Weaker components separate the main concentrations of H I in regions A, B, and C. We fit thirteen components to the Lyα–Lyϵ transitions for this absorption structure (Fig. 2, right). Their column densities are listed in Table 2, along with the velocity offset relative to the BG-C component redshift. Three components, FG-A1, FG-A2, and FG-B, are in the LLS range, with log N(H I) = 18.5, 18.6, and 18.8 respectively, all with $\sigma_{N(\text{H I})} \simeq 0.2$. The remaining ten components are all below log N(H I) = 16.0. The highest column density components, FG-A1, FG-A2, and FG-B, are aligned with strong absorptions in regions A and B of the BG quasar LOS (Fig. 3). The FG-A1 component is between the BG-A1 and BG-A2 components, whereas FG-A2 is exactly aligned with BG-A2 and FG-B is offset from BG-B by less than 35 km s^{-1}. In region C, three lower column density components with log N(H I) ≃ 14.8, 15.9, and 15.8 occur within 200 km s^{-1} of the BG-C sub-DLA.

3.2.2. Abundances

Low-ionization metals are detected only for the FG-A2 H I component (Fig. 5). The C II, Si II, Al II, and Fe II absorptions are fitted with two components, as required to follow the C II profile. The absorptions are weak, however, and often difficult to distinguish from the noise. Upper limits on the abundances are [C/H] ≤ −0.70 ± 0.48, [Si/H] ≤ −0.48 ± 0.40, [Al/H] ≤ −0.50 ± 0.45, and [Fe/H] ≤ −1.08 ± 0.47. Since the FG-A2 H I column density is log N(H I) = 18.6, the gas is not predominantly neutral and ionization corrections are likely significant. Both C II and Si II can be associated with the ionized gas.

To obtain a reliable metallicity indicator, we estimate an upper limit of log N(O I) ≤ 13.5 ± 0.1 for the three LLS, FG-A1, FG-A2, and FG-B, using the same process as in Section 3.1.2. Their corresponding metallicity limits are [O/H] ≤ −1.7, −1.8, and −2.0.

4. Discussion and conclusions

We studied coincident H I absorptions that occur in LOSs toward the FG and BG quasars in the J0913-0107 pair. Samples of close quasar pairs have been employed to measure quasar clustering when the redshift differences are negligible (e.g., Hennawi et al. 2010) and to investigate quasar host galaxy environments when

Table 3. Abundances relative to solar values (taken from Lodders 2003) for the log $N(\mathrm{H\,I})$ (cm^{-2}) > 18.0 absorption systems detected along the BG and FG quasar LOSs.

Comp.	v (km s^{-1})	$N(\mathrm{H\,I})$	$\sigma_{N(\mathrm{H\,I})}$	O	σ_{O}	Si	σ_{Si}	C	σ_{C}	Al	σ_{Al}	Fe	σ_{Fe}
BG-A1	−1681	19.90	0.06	−1.19	0.34	−1.57	0.11	−1.83	0.59	−2.06	0.15	−1.86	0.14
BG-A2	−1431	19.67	0.26	−1.56	0.43	−2.06	0.34	−2.10	0.34	−2.22	0.35	−2.35	0.30
BG-B	−834	18.41	0.23	≤−1.80	0.25	−	−	−	−	−	−	−	−
BG-C	0	20.15	0.05	−	−	−0.72	0.11	−	−	−0.89	0.08	−1.13	0.18
FG-A1	−1550	18.46	0.21	≤−1.65	0.24	−	−	−	−	−	−	−	−
FG-A2	−1432	18.57	0.24	≤−1.76	0.27	−	−	−	−	−	−	−	−
FG-B	−800	18.77	0.20	≤−1.96	0.23	−	−	−	−	−	−	−	−

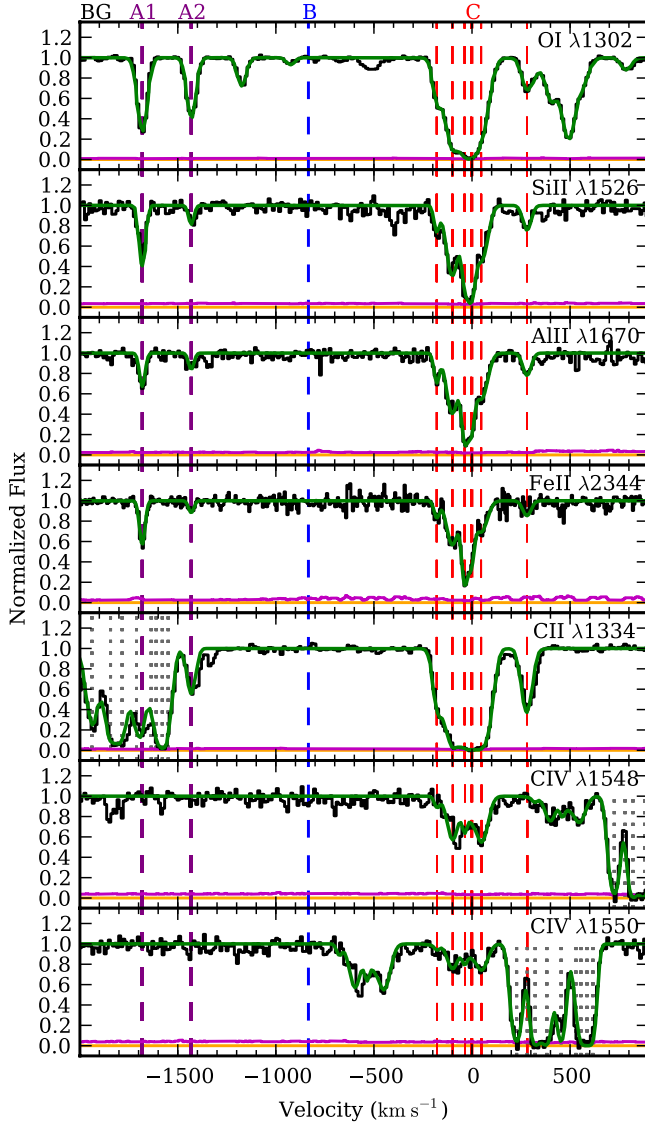**Notes.** Zero velocity corresponds to $z = 2.6894$.

Fig. 4. Fits to metal absorption lines in the BG quasar spectrum. Dashed purple, blue, and red lines mark components in regions A, B, and C. Thin dashed red lines indicate the six individual low-ionization components associated with region C. C IV absorptions are not detected for the BG-A1 and BG-A2 components, and no metal absorption lines associated with the BG-B component are detected. Si II λ1304 absorptions appear directly to the right of the O I λ1302 absorptions in the uppermost panel. The BG-A1 C II component is blended with the Si II λ1304 absorption from a $z \simeq 2.75$ DLA (dotted gray lines), but the BG-A2 component is unaffected. Dotted gray lines in the C IV $\lambda\lambda$1548, 1550 panels likewise indicate components from the Si II λ1526 absorption associated with the same $z \simeq 2.75$ DLA. Zero velocity is at $z = 2.6894$, and the 1-σ error on the flux is shown in magenta.
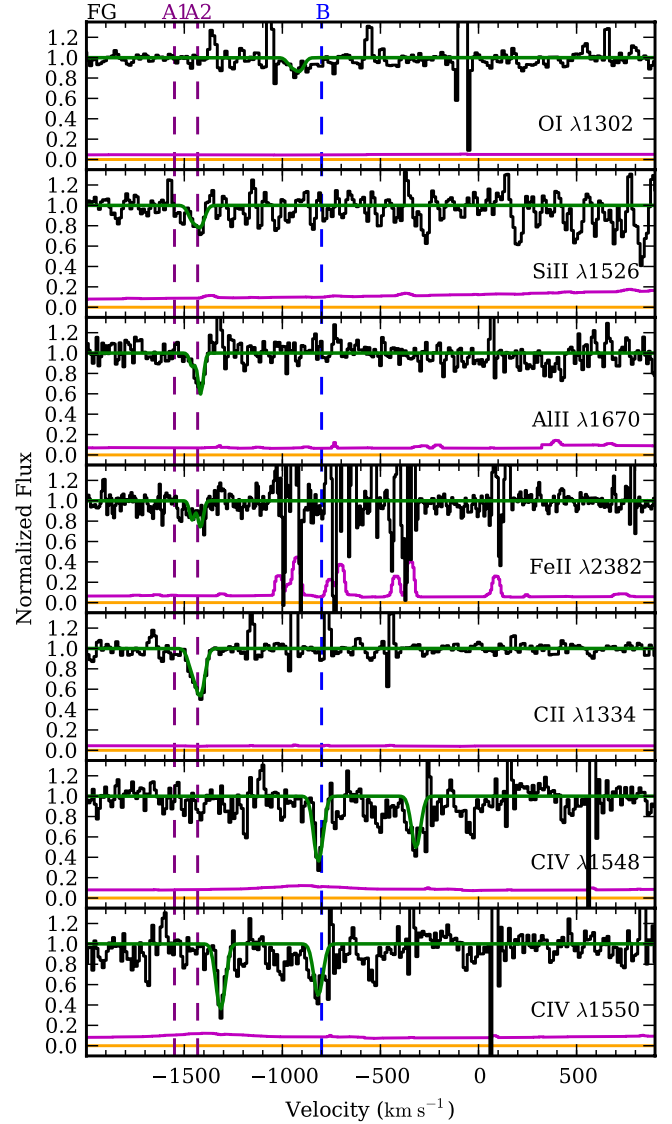
Fig. 5. Fits to metal absorption lines in the FG quasar spectrum. Dashed purple and blue lines mark the strong H I components in regions A and B. Weak low-ionization transitions (C II, Si II, Al II, Fe II) associated with FG-A2 are fitted with two components. No C IV is detected in region A to a limit of log $N(\mathrm{C\,IV})$ < 13.2 ± 0.1. For FG-B, only C IV is detected. Zero velocity is at $z = 2.6894$, and the 1-σ error on the flux is shown in magenta.

the redshifts are offset (e.g., Prochaska et al. 2013). Despite growing statistics, very few strong coincident absorptions along the LOSs have been reported. Ellison et al. (2007) analyzed a binary quasar pair featuring coincident DLA/sub-DLA systems

at both $z = 2.66$ and $z = 2.94$ along the two LOSs. The transverse distance between these LOSs, $\sim110\ h_{70}^{-1}$ kpc, is very similar to that of the LOSs presented here; however, the separation between the absorbers along the LOSs is an order of magnitude larger than the extent of the coincident absorption region in the J0913-0107 pair. The absorbers also have high [Zn/H] abundances. After comparing with cosmological simulations, the authors determined that the coincident absorptions are more likely due to groups of two or more galaxies than individual large galaxies.

In this work, the velocity separations, metallicities, and kinematics for coincident H I absorptions along the studied region in the two J0913-0107 quasar spectra suggest that their LOSs probe the same extended gaseous structure. As can be seen in Fig. 3, the absorption system kinematics and metallicities remain similar across the $\sim90\ h_{70}^{-1}$ kpc proper ($0.32\ h_{70}^{-1}$ Mpc comoving) distance separating the two LOSs. The highest column density absorptions in the FG LOS all have $\log N(\text{H\,\textsc{i}}) > 18.5$ counterparts in the BG LOS. The main exception is that the $\log N(\text{H\,\textsc{i}}) = 20.2$ BG-C component does not correspond to a high $N(\text{H\,\textsc{i}})$ absorption in the FG LOS.

In region A, the dense gas extends more than $90\ h_{70}^{-1}$ kpc in the transverse direction and 250 km s^{-1} along the LOSs. The components, which have [O/H] ≤ -1.7 (FG) and [C/O] $\sim$ [Fe/O] ~ -0.5 (BG), are consistent with very metal poor gas (Dutta et al. 2014) and approach what is believed to be the IGM metallicity (Simcoe et al. 2004). Each LOS has one strong component in region B. BG-B and FG-B are closely aligned and also have low metal abundances: [O/H] ≤ -1.8 and -2.0, respectively. Finally, the $\log N(\text{H\,\textsc{i}}) \simeq 20.2$ sub-DLA in region C with [Si/H] $= -0.7$ is likely associated with a galaxy. The BG-C abundance is somewhat higher than that of DLAs at the same redshift (Rafelski et al. 2012). If the BG-C sub-DLA galaxy is accreting gas from its surroundings, this could explain the lack of higher column density absorptions in region C of the FG spectrum. Due to accretion, gas in the galaxy halo becomes more sparsely distributed. The A, B, and C regions have distinct properties that are overall consistent in both spectra, but along each LOS the clouds do not appear to be directly in contact.

These absorptions span more than 1700 km s^{-1} along each LOS, which corresponds to a proper distance of $6.4\ h_{70}^{-1}$ Mpc at $z = 2.69$ ($23.6\ h_{70}^{-1}$ Mpc comoving). Velocity differences at this scale are dominated by the Hubble flow, rather than physical velocities intrinsic to the gas clouds. The A, B, and C absorption regions have a velocity separation of more than 5000 km s^{-1} from the FG quasar at $z = 2.75$, which makes direct association with the quasar environment unlikely (Ellison et al. 2010).

In addition to the $\log N(\text{H\,\textsc{i}}) > 18.0$ components, several weaker absorptions within the ~2000 km s^{-1} region are common to both LOSs. Corresponding absorptions with $\log N(\text{H\,\textsc{i}}) = 14.5-15.2$ occur near -1180 km s^{-1}, -720 km s^{-1}, and -450 km s^{-1}. For Lyα forest absorptions in the range $\log N(\text{H\,\textsc{i}}) = [14, 17]$ at $z \sim 2.55$, Kim et al. (2013) measured a mean line density dN/d$z = 76.38 \pm 7.32$. The regions where such Lyα absorptions can be detected in both LOSs cover a total of 950 km s^{-1}. This is less than the full coincident region, since the $\log N(\text{H\,\textsc{i}}) > 18.0$ systems completely absorb the flux in the remaining portion of the coincident region. The expected number of low column density absorptions is therefore 0.89 ± 0.09, whereas three are observed. The probability of such an occurrence is only 6%.

To investigate whether the strong absorption systems imply an overdensity, we evaluate the probability of finding two additional LLS within 2000 km s^{-1}, given that one LLS occurs

along the total path length. O'Meara et al. (2013) determined that the line density, dN/dz, for $\log N(\text{H\,\textsc{i}}) \geq 17.2$ cm^{-2} absorptions is 0.92 ± 0.18. For the redshift path between the BG quasar at $z = 2.916$ and the end of the spectrum at 3000 Å ($z = 1.468$), this probability is $\sim0.07\%$. Since the LLS absorptions in the J0913-0107 spectrum all have $\log N(\text{H\,\textsc{i}}) \geq 18.0$, the $\sim0.07\%$ probability can be considered an upper limit. The LOSs clearly probe an overdense region, which may be evidence of a galaxy protocluster, perhaps with a filamentary structure, or a filament in the IGM. We present arguments for the two interpretations.

Following hierarchical structure formation, regions that give rise to galaxy clusters at $z < 1$ have been matter-rich throughout cosmic time. In cosmological simulations, individual galaxies come together along gaseous filaments, creating small groups that in turn merge to form clusters by low redshift. Identifying overdense regions at high redshift that will eventually collapse to form gravitationally bound clusters at $z = 0$ is of particular interest for investigating galaxy cluster evolution. By tracking cluster formation in cosmological simulations, Chiang et al. (2013) were able to predict the $z = 0$ cluster mass from the galaxy overdensity at $2 < z < 5$. The comoving length of the coincident absorption region along the J0913-0107 LOSs is consistent with the expected effective diameter for a protocluster. However, to be identified as a protocluster at $z \sim 2-3$ with 80% confidence, a (25 Mpc comoving)^3 region must exhibit an overdensity of more than twice as many galaxies with $M_* > 10^9\ M_\odot$ than a typical field.

We consider whether is it likely that the absorbers probe gas in the environment of massive galaxies. Rahmati & Schaye (2014) associated $\log N(\text{H\,\textsc{i}}) > 17$ absorptions with galaxies in cosmological, hydrodynamical simulations (see also McQuinn et al. 2011) at $z = 3$ and found that most strong absorbers are most closely related to low mass galaxies with $M_* < 10^8\ M_\odot$. Only $\log N(\text{H\,\textsc{i}}) > 21$ absorptions are routinely associated with $M_* > 10^9\ M_\odot$ galaxies. The mass-metallicity relation similarly suggests that typical DLAs have $M_* \sim 10^{8.5}\ M_\odot$ (Møller et al. 2013). Although the A, B, and C regions in the J0913-0107 LOSs are overdense, the galaxies may not be sufficiently massive to directly contribute to the protocluster criterion.

Each quasar LOS can potentially detect C IV gas associated with the circumgalactic medium of massive star-forming galaxies out to a distance of $0.42\ h_{70}^{-1}$ Mpc comoving (Martin et al. 2010). Combining the Schechter mass function for field galaxies (Tomczak et al. 2014) with the factor of 2.2 overdensity necessary for a galaxy protocluster (Chiang et al. 2013), the LOSs probe a volume that would encompass only $\sim0.1\ M_* > 10^9\ M_\odot$ protocluster galaxies if they are randomly distributed. The possibility that the overdense region intersects a protocluster therefore cannot be ruled out, even if the absorber galaxies are not particularly massive. However, the overdensity of $\log N(\text{H\,\textsc{i}}) > 18$ absorbers is ~90, which is much higher than the expected overdensity of galaxies in a protocluster. This suggests that the absorbers could be aligned in a filamentary structure.

Cosmic web filaments are expected to consist of clumpy, moderate column density gas distributed over cosmological scales (e.g., Colberg et al. 2005; Cautun et al. 2014; see also Rasera & Teyssier 2006; Dubois et al. 2014, for examples of gaseous filaments in hydrodynamical simulations), much like the clouds diagrammed in Fig. 3. Furthermore, the process of mass build-up that results in galaxy clusters at low redshift is thought to occur along filamentary structures. The metallicity distribution along the overdense A, B, and C regions may indicate a filamentary structure. Absorptions in regions A and B probe very metal poor gas; their metal abundances are nearly an

order of magnitude below that of the BG-C component. Lehner et al. (2013) identify a bimodality in the metallicity distribution of $z \lesssim 1$ LLS and argue that the low-metallicity ($\langle [X/\mathrm{H}] \rangle < -1.57 \pm 0.24$) population traces gas accreting along filaments. Similarly, Bouché et al. (2013) highlight the metallicity difference between a $z = 2.3$ star-forming galaxy and gas detected in a DLA at an impact parameter of 26 kpc. The metallicity and gas kinematics of this system are consistent with a scenario where infalling IGM gas co-rotates in the halo before accreting onto the galaxy disk. The gas in the overdense region may be distributed along the length of a filament, probed by the two parallel quasar LOSs.

The observed substructures are likely not in interaction, based on the C IV content of the gas. In an environment where galaxies are interacting, we expect C IV to be conspicuous both because of metal enrichment and higher temperatures. Relatively little C IV absorption associated with the overdense H I region is apparent in the spectra (Figs. 4 and 5), and the C IV absorption associated with the BG-C sub-DLA is relatively weak. Consistent with the metallicity results, the lack of strong C IV absorption implies that the overdense region is not highly enriched. With high resolution, high signal-to-noise spectra, Songaila & Cowie (1996) studied the correspondance between H I and C IV absorptions. They found that 90% of log $N(\mathrm{H\,I}) > 15.2$ absorptions have log $N(\mathrm{C\,IV}) > 12.0$. In the range log $N(\mathrm{H\,I}) = [15, 17]$, the median C IV/H I value is 3×10^{-3}. The detection limit of log $N(\mathrm{C\,IV}) < 12.8$ (BG) and 13.2 (FG) may nevertheless be insufficient to reveal C IV absorptions associated with the lower column density H I components.

We favor the interpretation that the gas is distributed in a 6.4 h_{70}^{-1} Mpc proper filament at $z \simeq 2.69$. The high concentration of gas clouds along the LOSs is difficult to explain with the factor of ~2 galaxy overdensity expected in a protocluster and suggests a clumpy, filamentary structure. The metallicities in regions A and B differ by a factor of ten from the metallicity in region C, and the lack of strong C IV absorption likewise implies that the overdense region is not highly enriched. However, we cannot rule out that this filamentary structure represents the first stages of cluster formation. Imaging this field to search for galaxies associated with the overdensity is essential to unveiling its true nature. Detecting a possible filament in absorption is a step forward in revealing the structure of the IGM on small scales and foreshadows what will be possible with the next generation of 30 m telescopes.

References

Aragón-Calvo, M. A., van de Weygaert, R., & Jones, B. J. T. 2010, MNRAS, 408, 2163
Bond, J. R., Kofman, L., & Pogosyan, D. 1996, Nature, 380, 603
Bond, N. A., Strauss, M. A., & Cen, R. 2010, MNRAS, 409, 156
Bouché, N., Murphy, M. T., Kacprzak, G. G., et al. 2013, Science, 341, 50
Cappetta, M., D'Odorico, V., Cristiani, S., Saitta, F., & Viel, M. 2010, MNRAS, 407, 1290
Caucci, S., Colombi, S., Pichon, C., et al. 2008, MNRAS, 386, 211
Cautun, M., van de Weygaert, R., Jones, B. J. T., & Frenk, C. S. 2014, MNRAS, 441, 2923
Chiang, Y.-K., Overzier, R., & Gebhardt, K. 2013, ApJ, 779, 127
Cisewski, J., Croft, R. A. C., Freeman, P. E., et al. 2014, MNRAS, 440, 2599
Colberg, J. M., Krughoff, K. S., & Connolly, A. J. 2005, MNRAS, 359, 272
Cooke, R., Pettini, M., Steidel, C. C., Rudie, G. C., & Nissen, P. E. 2011, MNRAS, 417, 1534
Coppolani, F., Petitjean, P., Stoehr, F., et al. 2006, MNRAS, 370, 1804
Dawson, K. S., Schlegel, D. J., Ahn, C. P., et al. 2013, AJ, 145, 10
D'Odorico, V., Cristiani, S., D'Odorico, S., et al. 1998, A&A, 339, 678
D'Odorico, V., Viel, M., Saitta, F., et al. 2006, MNRAS, 372, 1333
Dubois, Y., Pichon, C., Welker, C., et al. 2014, MNRAS, 444, 1453
Dutta, R., Srianand, R., Rahmani, H., et al. 2014, MNRAS, 440, 307
Eisenstein, D. J., Weinberg, D. H., Agol, E., et al. 2011, AJ, 142, 72
Ellison, S. L., Hennawi, J. F., Martin, C. L., & Sommer-Larsen, J. 2007, MNRAS, 378, 801
Ellison, S. L., Prochaska, J. X., Hennawi, J., et al. 2010, MNRAS, 406, 1435
Evans, C. J., Puech, M., Barbuy, B., et al. 2014, Proc. SPIE, 9147, 914796
Field, G. B., & Steigman, G. 1971, ApJ, 166, 59
Finley, H., Petitjean, P., Pâris, I., et al. 2013, A&A, 558, A111
González, R. E. & Padilla, N. D. 2010, MNRAS, 407, 1449
Hennawi, J. F., Myers, A. D., Shen, Y., et al. 2010, ApJ, 719, 1672
Jauzac, M., Jullo, E., Kneib, J.-P., et al. 2012, MNRAS, 426, 3369
Kelson, D. D. 2003, PASP, 115, 688
Kim, T.-S., Partl, A. M., Carswell, R. F., & Müller, V. 2013, A&A, 552, A77
Komatsu, E., Smith, K. M., Dunkley, J., et al. 2011, ApJS, 192, 18
Lee, K.-G., Hennawi, J. F., White, M., Croft, R. A. C., & Ozbek, M. 2014, ApJ, 788, 49
Lehner, N., Howk, J. C., Tripp, T. M., et al. 2013, ApJ, 770, 138
Lodders, K. 2003, ApJ, 591, 1220
Maiolino, R., Haehnelt, M., Murphy, M. T., et al. 2013 [arXiv:1310.3163]
Martin, C. L., Scannapieco, E., Ellison, S. L., et al. 2010, ApJ, 721, 174
McQuinn, M., Oh, S. P., & Faucher-Giguère, C.-A. 2011, ApJ, 743, 82
Mead, J. M. G., King, L. J., & McCarthy, I. G. 2010, MNRAS, 401, 2257
Modigliani, A., Goldoni, P., Royer, F., et al. 2010, in SPIE Conf. Ser., 7737, 28
Møller, P., Fynbo, J. P. U., Ledoux, C., & Nilsson, K. K. 2013, MNRAS, 430, 2680
Murphy, D. N. A., Eke, V. R., & Frenk, C. S. 2011, MNRAS, 413, 2288
Noterdaeme, P., Laursen, P., Petitjean, P., et al. 2012a, A&A, 540, A63
Noterdaeme, P., Petitjean, P., Carithers, W. C., et al. 2012b, A&A, 547, L1
O'Meara, J. M., Prochaska, J. X., Worseck, G., Chen, H.-W., & Madau, P. 2013, ApJ, 765, 137
Pandey, B., Kulkarni, G., Bharadwaj, S., & Souradeep, T. 2011, MNRAS, 411, 332
Pâris, I., Petitjean, P., Aubourg, É., et al. 2012, A&A, 548, A66
Prochaska, J. X., & Wolfe, A. M. 2002, ApJ, 566, 68
Prochaska, J. X., Hennawi, J. F., Lee, K.-G., et al. 2013, ApJ, 776, 136
Rafelski, M., Wolfe, A. M., Prochaska, J. X., Neeleman, M., & Mendez, A. J. 2012, ApJ, 755, 89
Rahmati, A., & Schaye, J. 2014, MNRAS, 438, 529
Rasera, Y., & Teyssier, R. 2006, A&A, 445, 1
Rollinde, E., Petitjean, P., Pichon, C., et al. 2003, MNRAS, 341, 1279
Rudie, G. C., Steidel, C. C., Trainor, R. F., et al. 2012, ApJ, 750, 67
Saitta, F., D'Odorico, V., Bruscoli, M., et al. 2008, MNRAS, 385, 519
Simcoe, R. A., Sargent, W. L. W., & Rauch, M. 2004, ApJ, 606, 92
Smith, A. G., Hopkins, A. M., Hunstead, R. W., & Pimbblet, K. A. 2012, MNRAS, 422, 25
Songaila, A., & Cowie, L. L. 1996, AJ, 112, 335
Sousbie, T., Pichon, C., & Kawahara, H. 2011, MNRAS, 414, 384
Steidel, C., Martin, C., Prochaska, J. X., et al. 2009, in astro2010: The Astronomy and Astrophysics Decadal Survey, 286
Tanaka, M., Hoshi, T., Kodama, T., & Kashikawa, N. 2007, MNRAS, 379, 1546
Tempel, E., Stoica, R. S., Martínez, V. J., et al. 2014, MNRAS, 438, 3465
Tomczak, A. R., Quadri, R. F., Tran, K.-V. H., et al. 2014, ApJ, 783, 85
van Dokkum, P. G. 2001, PASP, 113, 1420
Verdugo, M., Lerchster, M., Böhringer, H., et al. 2012, MNRAS, 421, 1949
Vladilo, G. 2002, A&A, 391, 407
York, D. G., Adelman, J., Anderson, Jr., J. E., et al. 2000, AJ, 120, 1579